INTERNATIONAL JOURNAL FOR NUMERICAL METHODS IN FLUIDS
Int. J. Numer. Meth. Fluids 2012; **69**:430–441
Published online 7 April 2011 in Wiley Online Library (wileyonlinelibrary.com/journal/nmf). DOI: 10.1002/fld.2567

Development of a convection–diffusion–reaction model for solving Maxwell's equations in frequency domain

Tony W. H. Sheu[1,2,3,*,†,‡], K. C. Lin[1] and J. H. Li[1]

[1]*Department of Engineering Science and Ocean Engineering, National Taiwan University, No. 1, Sec. 4, Roosevelt Road, Taipei 10617, Taiwan*
[2]*Taida Institute of Mathematical Science (TIMS), National Taiwan University, Taipei, Taiwan*
[3]*Center for Quantum Science and Engineering (CQSE), National Taiwan University, Taipei, Taiwan*

SUMMARY

We propose in this study a numerically accurate and computationally efficient convection–diffusion–reaction finite difference scheme to discretize the full-vector and semi-vector optical waveguide equations. The scheme formulated in a grid stencil of five nodal points for solving the three-dimensional waveguide equations employs the locally analytic solution. In this three-dimensional study, calculations were carried out for the investigation of wave propagation in diffused channel, rectangular and rib types of optical waveguide. Copyright © 2011 John Wiley & Sons, Ltd.

Received 5 November 2009; Revised 9 January 2011; Accepted 22 February 2011

KEY WORDS: convection–diffusion–reaction; full-vector; semi-vector; waveguide equations

1. INTRODUCTION

Demand on improving the integrated optical devices remains growing in optical communication society. Design of an ever-improving modulator, switch, filter, fiber and semiconductor laser in some geometrically complex settings has prompted scientists to resort to the high-performance simulation approach. For acquiring the precise propagation characteristics in an increasingly complex waveguide with possibly complex refractive index profiles, it is essential to analyze the Maxwell's equations, which theoretically govern the wave propagation in optical devices, by numerical simulations.

The computationally less intensive beam-propagating method (BPM) [1] can be applied to predict the forward-running wave without the consideration of wave reflection in the device. This approach can be, in particular, applicable to optical structures which allow only a very small refractive index change along the axial direction. One can also resort to the differential equation approach, which seeks direct solution to the Maxwell's equations, by solving the Faraday's and Ampère's equations in space as well as in time. Time-domain approaches have the advantage of simulating electromagnetic waves over a wide frequency range [2]. Preservation of the Hamiltonian property [3] and energy density in Maxwell's equations poses, however, an academic challenge regarding the calculation of a long-time accurate waveguide solution. The predicted solution may be doubtful unless the symplectic property embedded in Maxwell's equations is conserved all the

*Correspondence to: Tony W. H. Sheu, Department of Engineering Science and Ocean Engineering, National Taiwan University, No. 1, Sec. 4, Roosevelt Road, Taipei 10617, Taiwan.
†E-mail: twhsheu@ntu.edu.tw
‡Professor.

time [4]. In this study, frequency-domain approach will be chosen to avoid the approximation of time derivative terms. The intrinsic Hamiltonian can, as a result, be preserved all the time in the waveguide simulation.

Approximation of Maxwell's equations will inevitably introduce dissipation and dispersion errors. Dissipation error can attenuate wave amplitude and dispersion error can even cause the solution to blow up due to an erroneously predicted wave propagation speed. The computed wave attenuation and incorrect propagation speed are both considered as the obstacles of making an accurate design of waveguide devices. We are therefore motivated to develop a numerically very accurate and computationally less expensive frequency-domain waveguide solution solver. When solving the Maxwell's equations in frequency domain, it is essential to compute the resulting eigenvalues effectively. One can find a large body of literatures in [5] for computing the definite-frequency efficiently in arbitrary periodic dielectric structures.

The remainder of this paper is organized as follows. In Section 2, the waveguide equations cast in their full-vector, semi-vector, and scalar forms will be presented for the prediction of optical wave propagation. This is followed by presenting in Section 3 the convection–diffusion–reaction (CDR) finite difference scheme and in Section 4 the eigenvalue solver for the calculation of effective refractive index in the three-dimensional waveguide equations. Validation study of several problems will be presented in Section 5 to justify the integrity of the proposed scheme. In Section 6, some concluding remarks will be drawn.

2. WAVEGUIDE EQUATIONS

To predict the propagation characteristics in optical waveguides, we will numerically solve the three-dimensional Maxwell's equations for the EM field in a medium with spatially varying permittivity $\underline{\varepsilon}(\underline{x})$ and constant permeability μ. In the absence of free charges and electric currents, the magnetic field $\underline{H}$ and the electric field $\underline{E}$ are governed, respectively, by the following wave equations:

$$\partial \underline{H}/\partial t = \frac{-1}{\mu}\nabla \times \underline{E} \tag{1}$$

$$\partial \underline{E}/\partial t = \frac{1}{\varepsilon}\nabla \times \underline{H} \tag{2}$$

Faraday's law of conduction (or Equation (1)) and Ampère's law (or Equation (2)) are, in theory, constrained by the following Gauss's laws for the respective magnetism and electricity:

$$\nabla \cdot \underline{B} = 0 \tag{3}$$

$$\nabla \cdot \underline{D} = 0 \tag{4}$$

The above two field vectors $\underline{B}$ and $\underline{D}$ are known as the magnetic flux density and the electric flux density, respectively. To calculate the 12 unknown field variables from the 8 equations given (1)–(4), another 6 constitutive equations given below for the medium under current investigation are required for the closure of three-dimensional Maxwell's equations

$$\underline{B} = \mu \underline{H} \tag{5}$$

$$\underline{D} = \varepsilon \underline{E} \tag{6}$$

The two material properties μ and ε shown above determine the local speed of light c, which is expressed by $c = (\mu\varepsilon)^{-1/2}$.

Within the continuous context of differential equations, Maxwell's equations (1) and (4) are not independent of each other. One can perform the divergence operation on (1) and (2) to obtain Equations (3) and (4), respectively. This explains why the hyperbolic equations given in (1) and (2) are sufficient to close the EM fields for the six unknowns $\underline{H}$ and $\underline{E}$. In mathematics, if the initial solutions for the field variables $\underline{E}$ and $\underline{H}$ are divergence-free, the time-evolving equations given in

DOI: 10.1002/fld

(1) and (2) will automatically satisfy the divergence-free conditions given in (3) and (4) all the time [6]. In practice, the predicted solution should satisfy the divergence-free conditions exactly or very accurately in the discrete sense. This necessity poses, however, a great challenge computationally. From the mathematical point of view, omission of the divergence-free equations (3) and (4) in the course of conducting EM wave simulation will deteriorate the ellipticity of Maxwell's equations [7]. This implies that the negligence of two zero-divergence constraints may be accompanied with a serious defect. In recognition of this computational difficulty, we are motivated to develop a very accurate scheme by solving Maxwell's equations in frequency domain. In other words, numerical simulation of Maxwell's equations in frequency domain is considered as the compensation of the omitted Gauss's laws for magnetism and electricity.

Provided that an electromagnetic wave is propagated along the z-direction in a time dependence fashion given by $\exp(\mathrm{j}\omega t)$ in a medium having the spatially varied refractive index $n(\underline{x})$, Equations (1)–(4) can be transformed into the following equations in frequency domain under the condition of specifying the constant values of μ and ε, which are μ_0 and ε_0 [8]:

$$\nabla \times \underline{E} = -\mathrm{j}\omega\mu_0 \underline{H} \tag{7}$$

$$\nabla \times \underline{H} = \mathrm{j}\omega\varepsilon_0 n^2 \underline{E} \tag{8}$$

$$\nabla \cdot (\varepsilon_0 n^2 \underline{E}) = 0 \tag{9}$$

$$\nabla \cdot (\mu_0 \underline{H}) = 0 \tag{10}$$

By performing the curl operator on Equation (7), the wave equation given below for the electric field can be derived in frequency domain thanks to Equations (8) and (9)

$$\nabla^2 \underline{E} + k_0{}^2 n^2 \underline{E} + \nabla\left(\frac{\nabla n^2}{n^2} \cdot \underline{E}\right) = 0 \tag{11}$$

We can also derive the wave equation given below for the magnetic field in frequency domain by performing the curl operator on Equation (8) and using Equations (7), (8) and (10)

$$\nabla^2 \underline{H} + k_0{}^2 n^2 \underline{H} + \frac{\nabla n^2}{n^2} \times (\nabla \times \underline{H}) = 0 \tag{12}$$

In the above equation, k_0 is equal to $2\pi/\lambda_0$, where λ_0 is the wavelength in free space.

For a longitudinally invariant optical structure, $\partial n/\partial z$ is equal to zero along the z-direction. The refractive index n will be varied solely along the transverse directions x and y, implying that $n = n(x, y)$. The following equations with the mode that is periodic z-dependence (or $\exp(-\mathrm{j}\beta z)$) will be under current investigation:

$$\frac{\partial}{\partial x}\left(\frac{1}{n^2}\frac{\partial n^2}{\partial x}E_x\right) + \left(\frac{\partial^2 E_x}{\partial x^2} + \frac{\partial^2 E_x}{\partial y^2}\right) + k_0^2(n^2 - n_{\mathrm{e}}^2)E_x + \frac{\partial}{\partial x}\left(\frac{1}{n^2}\frac{\partial n^2}{\partial y}E_y\right) = 0 \tag{13}$$

$$\frac{\partial}{\partial y}\left(\frac{1}{n^2}\frac{\partial n^2}{\partial y}E_y\right) + \left(\frac{\partial^2 E_y}{\partial x^2} + \frac{\partial^2 E_y}{\partial y^2}\right) + k_0^2(n^2 - n_{\mathrm{e}}^2)E_y + \frac{\partial}{\partial y}\left(\frac{1}{n^2}\frac{\partial n^2}{\partial x}E_x\right) = 0 \tag{14}$$

$$-\frac{1}{n^2}\frac{\partial n^2}{\partial y}\frac{\partial H_x}{\partial y} + \left(\frac{\partial^2 H_x}{\partial x^2} + \frac{\partial^2 H_x}{\partial y^2}\right) + k_0^2 n^2 H_x = k_0^2 n_{\mathrm{e}}^2 H_x - \frac{1}{n^2}\frac{\partial n^2}{\partial y}\frac{\partial H_y}{\partial x} \tag{15}$$

$$-\frac{1}{n^2}\frac{\partial n^2}{\partial x}\frac{\partial H_y}{\partial x} + \left(\frac{\partial^2 H_y}{\partial x^2} + \frac{\partial^2 H_y}{\partial y^2}\right) + k_0^2 n^2 H_y = k_0^2 n_{\mathrm{e}}^2 H_y - \frac{1}{n^2}\frac{\partial n^2}{\partial x}\frac{\partial H_x}{\partial y} \tag{16}$$

In the above equation, the effective refractive index $n_{\mathrm{e}}(=(1/k_0)\beta)$ is proportional to the propagation constant β. Equations (13), (14) and (15), (16) are called the full-vector waveguide equations for the electric and magnetic fields, respectively.

DOI: 10.1002/fld

In this paper, we will solely simulate magnetic field, which is governed by Equations (15) and (16). Calculation of these two equations, which are cast in the inhomogeneous CDR form, needs to determine the effective refractive index n_e and propose the inhomogeneous CDR scheme for the spatial derivatives. For this reason, we will present the two-dimensional CDR scheme in Section 3 for the discretization of Equations (15) and (16) and then in Section 4 for the determination of n_e.

3. CONVECTION–DIFFUSION–REACTION SCHEME

In the frequency domain, the waveguide Equations (15) and (16) in (x, y) domain take the time-independent CDR differential form. We will therefore employ the following two-dimensional inhomogeneous equation as the model equation to describe the discretization method for the investigated waveguide equations:

$$u\phi_x + v\phi_y - k\nabla^2\phi + c\phi = f \tag{17}$$

In what follows, the values of u, v, k and c are assumed to be constant for the description of the proposed CDR scheme given below. In Equation (17), $f = k_0^2 n_e^2 H_x - ((1/n^2)(\partial n^2/\partial y))(\partial H_y/\partial x)$ for Equation (15) and $f = k_0^2 n_e^2 H_y - ((1/n^2)(\partial n^2/\partial x))(\partial H_x/\partial y)$ for Equation (16). In this study, we are aimed to obtain the solution with higher accuracy by employing the following general solution for Equation (17):

$$\phi(x, y) = A_1 e^{\lambda_1 x} + A_2 e^{\lambda_2 x} + A_3 e^{\lambda_3 y} + A_4 e^{\lambda_4 y} + \frac{f}{c} \tag{18}$$

In the above equation, A_1–A_4 are the four constants. By substituting Equation (18) into Equation (17), λ_1–λ_4 can be derived as follows in [9]:

$$\lambda_{1,2} = \frac{u \pm \sqrt{u^2 + 4ck}}{2k} \quad \text{and} \quad \lambda_{3,4} = \frac{v \pm \sqrt{v^2 + 4ck}}{2k} \tag{19}$$

For the model equation (17), we can write the discrete equation at an interior node (i, j) in terms of the numerical diffusion coefficient m as follows:

$$\frac{u}{2h}(\phi_{i+1,j} - \phi_{i-1,j}) + \frac{v}{2h}(\phi_{i,j+1} - \phi_{i,j-1}) - \frac{m}{h^2}(\phi_{i+1,j} + \phi_{i-1,j} - 4\phi_{i,j} + \phi_{i,j+1} + \phi_{i,j-1})$$
$$+ \frac{c}{12}(\phi_{i+1,j} + \phi_{i-1,j} + 8\phi_{i,j} + \phi_{i,j+1} + \phi_{i,j-1}) = f_{i,j} \tag{20}$$

Note that the derivative terms ϕ_x, ϕ_y, ϕ_{xx}, ϕ_{yy} and the unknown ϕ are all approximated by the center schemes with the replacement of the physical diffusivity k in Equation (17) by its numerical counterpart m, which will be determined below to enhance scheme stability and improve numerical accuracy. Equation (20) can be further rewritten to the following five-stencil discrete form:

$$\left(-\frac{u}{2h} - \frac{m}{h^2} + \frac{c}{12}\right)\phi_{i-1,j} + \left(\frac{u}{2h} - \frac{m}{h^2} + \frac{c}{12}\right)\phi_{i+1,j} + 4\left(\frac{m}{h^2} + \frac{2c}{12}\right)\phi_{i,j}$$
$$+ \left(-\frac{v}{2h} - \frac{m}{h^2} + \frac{c}{12}\right)\phi_{i,j-1} + \left(\frac{v}{2h} - \frac{m}{h^2} + \frac{c}{12}\right)\phi_{i,j+1} = f_{i,j} \tag{21}$$

In the above equation, h is the uniform grid size.

Given the above discrete representation, which is Equation (21) for the model equation (17), the prediction quality depends solely on the introduced diffusion coefficient m. By virtue of Equation (18), the exact solutions given by $\phi_{i,j} = A_1 e^{\lambda_1 x_i} + A_2 e^{\lambda_2 x_i} + A_3 e^{\lambda_3 y_j} + A_4 e^{\lambda_4 y_j} + (f/c)$, $\phi_{i\pm1,j} = A_1 e^{\pm\lambda_1 h} e^{\lambda_1 x_i} + A_2 e^{\pm\lambda_2 h} e^{\lambda_2 x_i} + A_3 e^{\lambda_3 y_j} + A_4 e^{\lambda_4 y_j} + (f/c)$ and $\phi_{i,j\pm1} = A_1 e^{\lambda_1 x_i} + A_2 e^{\lambda_2 x_i} + A_3 e^{\pm\lambda_3 h} e^{\lambda_3 y_j} + A_4 e^{\pm\lambda_4 h} e^{\lambda_4 y_j} + (f/c)$ are substituted into Equation (21). This substitution

DOI: 10.1002/fld

of the nodal exact solutions enables us to obtain the expression for the coefficient m shown in (21) as follows [9]:

$$m=\left[\frac{uh}{2}\sinh\overline{\lambda}_1\cosh\overline{\lambda}_2+\frac{vh}{2}\sinh\overline{\lambda}_3\cosh\overline{\lambda}_4+\frac{ch^2}{12}(\cosh\overline{\lambda}_1\cosh\overline{\lambda}_2+\cosh\overline{\lambda}_3\cosh\overline{\lambda}_4+10)\right]\Big/$$
$$(\cosh\overline{\lambda}_1\cosh\overline{\lambda}_2+\cosh\overline{\lambda}_3\cosh\overline{\lambda}_4-2) \tag{22}$$

In the above equation

$$(\overline{\lambda}_1,\overline{\lambda}_2)=\left(\frac{uh}{2k},\sqrt{\left(\frac{uh}{2k}\right)^2+\frac{ch^2}{k}}\right)\quad\text{and}\quad(\overline{\lambda}_3,\overline{\lambda}_4)=\left(\frac{vh}{2k},\sqrt{\left(\frac{vh}{2k}\right)^2+\frac{ch^2}{k}}\right)$$

4. DETERMINATION OF H_x AND H_y

Define the coefficients u, v, k, c shown in Equation (17) as $u=0$, $v=-(1/n^2)(\partial n^2/\partial y)$, $k=-1$, $c=k_0^2n^2$. Given that $f=k_0^2n_e^2H_x-((1/n^2)(\partial n^2/\partial y))(\partial H_y/\partial x)$, we can then apply the CDR scheme proposed in the previous section to approximate Equation (15) in a grid of five stencil points. The resulting discrete equation is given below

$$(a_1)_{i,j}H_x|_{i,j-1}+(a_2)_{i,j}H_x|_{i-1,j}+(a_3)_{i,j}H_x|_{i,j}+(a_4)_{i,j}H_x|_{i+1,j}+(a_5)_{i,j}H_x|_{i,j+1}=f_{i,j} \tag{23}$$

where $(a_1)_{i,j}=-(v_{i,j}/2h)-(m_{i,j}/h^2)+(c_{i,j}/12)$, $(a_2)_{i,j}=-(u_{i,j}/2h)-(m_{i,j}/h^2)+(c_{i,j}/12)$, $(a_3)_{i,j}=(m_{i,j}/h^2)+(2c_{i,j}/12)$, $(a_4)_{i,j}=(u_{i,j}/2h)-(m_{i,j}/h^2)+(c_{i,j}/12)$ and $(a_5)_{i,j}=(v_{i,j}/2h)-(m_{i,j}/h^2)+(c_{i,j}/12)$. By substituting the following second-order accurate approximated equation:

$$-\frac{1}{n^2}\frac{\partial n^2}{\partial y}\frac{\partial H_y}{\partial x}=(e_1)_{i,j}\left\{\equiv\left(-\frac{1}{n^2}\frac{\partial n^2}{\partial y}\right)_{i,j}\right\}H_y\Big|_{i-1,j}-(e_2)_{i,j}\left\{\equiv\left(-\frac{2}{n^2}\frac{\partial n^2}{\partial y}\right)_{i,j}\right\}H_y\Big|_{i,j}$$
$$+(e_3)_{i,j}\left\{\equiv\left(-\frac{1}{n^2}\frac{\partial n^2}{\partial y}\right)_{i,j}\right\}H_y\Big|_{i+1,j} \tag{24}$$

into Equation (23), we are led to derive

$$(a_1)_{i,j}H_x|_{i,j-1}+(a_2)_{i,j}H_x|_{i-1,j}+(a_3)_{i,j}H_x|_{i,j}+(a_4)_{i,j}H_x|_{i+1,j}+(a_5)_{i,j}H_x|_{i,j+1}$$
$$+(e_1)_{i,j}H_y|_{i-1,j}+(e_2)_{i,j}H_y|_{i,j}+(e_3)_{i,j}H_y|_{i+1,j}=k_0^2n_e^2H_x|_{i,j} \tag{25}$$

For Equation (16), it can be similarly approximated as follows:

$$(b_1)_{i,j}H_y|_{i,j-1}+(b_2)_{i,j}H_y|_{i-1,j}+(b_3)_{i,j}H_y|_{i,j}+(b_4)_{i,j}H_y|_{i+1,j}+(b_5)_{i,j}H_y|_{i,j+1}$$
$$+(f_1)_{i,j}H_x|_{i-1,j}+(f_2)_{i,j}H_x|_{i,j}+(f_3)_{i,j}H_x|_{i+1,j}=k_0^2n_e^2H_y|_{i,j} \tag{26}$$

where $(b_1)_{i,j}=-(v_{i,j}/2h)-(m_{i,j}/h^2)+(c_{i,j}/12)$, $(b_2)_{i,j}=-(u_{i,j}/2h)-(m_{i,j}/h^2)+(c_{i,j}/12)$, $(b_3)_{i,j}=(m_{i,j}/h^2)+(2c_{i,j}/12)$, $(b_4)_{i,j}=(u_{i,j}/2h)-(m_{i,j}/h^2)+(c_{i,j}/12)$, $(b_5)_{i,j}=(v_{i,j}/2h)-(m_{i,j}/h^2)+(c_{i,j}/12)$, and $(f_k)_{i,j}=(v_{i,j}/2h)-(m_{i,j}/h^2)+(c_{i,j}/12)$, $k=1,2,3$.

The above two algebraic equations can be cast in the following matrix form:

$$[A]_{(2N\times M)\times(2N\times M)}\begin{bmatrix}H_x\\H_y\end{bmatrix}_{(2N\times M)\times(N\times M)}\equiv[\lambda]_{(2N\times M)\times(2N\times M)}\begin{bmatrix}H_x\\H_y\end{bmatrix}_{(2N\times M)\times(N\times M)} \tag{27}$$

DOI: 10.1002/fld

where N and M represent the number of mesh points along the x-axis and y-axis, respectively. Note that $\underline{\underline{\lambda}}$ ($\equiv$diag$\{\lambda_1, \lambda_2, \ldots, \lambda_{(2N\times M)}\}$), $\underline{\underline{X}}$ ($\equiv[H_x H_y]^{\mathrm{T}}$) and

$$[A]=\begin{bmatrix}(A_1)_{(N\times M)\times(2N\times M)}\\(A_2)_{(N\times M)\times(2N\times M)}\end{bmatrix}_{(2N\times M)\times(2N\times M)} \tag{28}$$

The components A_1 in the above matrix are expressed as $(A_1)_{r_1,r_1-N}=(a_1)_{i,j}$, $(A_1)_{r_1,r_1-1}=(a_2)_{i,j}$, $(A_1)_{r_1,r_1}=(a_3)_{i,j}$, $(A_1)_{r_1,r_1+1}=(a_4)_{i,j}$, $(A_1)_{r_1,r_1+N}=(a_5)_{i,j}$, $(A_1)_{r_1,r_1+N\cdot M-1}=(e_1)_{i,j}$, $(A_1)_{r_1,r_1+N\cdot M}=(e_2)_{i,j}$, $(A_1)_{r_1,r_1+N\cdot M+1}=(e_3)_{i,j}$, where $r_1=i+(j-1)N$. As for the components of A_2 in the matrix shown in (28), they can be similarly derived as $(A_2)_{r_2,r_2-N}=(b_1)_{i,j}$, $(A_2)_{r_2,r_2-1}=(b_2)_{i,j}$, $(A_2)_{r_2,r_2}=(b_3)_{i,j}$, $(A_2)_{r_2,r_2+1}=(b_4)_{i,j}$, $(A_2)_{r_2,r_2+N}=(b_5)_{i,j}$, $(A_2)_{r_2,r_2-N\cdot M-N}=(f_1)_{i,j}$, $(A_2)_{r_2,r_2-N\cdot M}=(f_2)_{i,j}$, $(A_2)_{r_2,r_2-N\cdot M+N}=(f_3)_{i,j}$, where $r_2=i+(j-1)N+(N\cdot M)$.

From the eigenvalue equation $\underline{\underline{A}}\,\underline{\underline{X}}=\underline{\underline{\lambda}}\,\underline{\underline{X}}$, we apply Matlab to compute the eigenvalues from the diagonal matrix $\underline{\underline{\lambda}}$ and then the solution matrix $\underline{\underline{X}}$. Amongst the predicted eigenvalues $\{\lambda_1, \lambda_2, \ldots, \lambda_{(2N\times M)}\}$, only the eigenvalues ($\lambda_i=k_0^2 n_{\mathrm{e}_i}^2$, $i=1, 2, 3, \ldots, 2N\times M$) within the range of $k_0^2 n_{\mathrm{cladding}}^2$ and $k_0^2 n_{\mathrm{core}}^2$ will be under investigation. Starting from the largest eigenvalue, we can calculate the corresponding fundamental mode solution. This is followed by employing the rest of the smaller eigenvalues to get their corresponding eigenvectors.

5. NUMERICAL RESULTS

The proposed CDR scheme will be first justified through the following two-dimensional constant-coefficient scalar equation in a square domain $0\leqslant x, y\leqslant 1$:

$$a\phi_x+b\phi_y+c\nabla^2\phi+d\phi=f \tag{29}$$

This equation is amenable to the exact solution given by $\phi_{\mathrm{exact}}=\sin x\cos y$ provided that f is chosen as $f=\cos x\cos y-\sin x\sin y+2\sin x\cos y$. Solutions will be computed at $a=1$, $b=1$, $c=-1$ and $d=0$ in the five chosen grids with the uniform mesh sizes of $h=0.1$, 0.05, 0.025, 0.0125, 0.00625. The computed errors cast in their L_2-error norms are then plotted against the grid size of $\Delta x=\Delta y=h$ in Figure 1. These computed errors are seen to decrease with the decreasing grid sizes at an approximated rate of 1.955, thereby confirming the integrity of the proposed two-dimensional CDR scheme. Having justified the employed CDR scheme, which will be used to approximate the waveguide equations in three-dimensional waveguide structures, we will consider below the problems with the spatially varying refractive index profiles.

The first three-dimensional problem under current investigation is the optical wave propagation in the diffused channel schematic in Figure 2. The refractive index profile in this waveguide is the result of diffusing Ti^{+2} into $LiNbO_3$ in the x–y plane, thereby yielding the graded profile given below [10]

$$n(x, y)=\begin{cases}[n_s{}^2+2n_s\Delta n f(y)g(x)]^{1/2}, & y\geqslant 0\\ n_c, & y<0\end{cases} \tag{30}$$

where $f(y)=((\mathbf{erf}[(y+a)/\sqrt{2}D]-\mathbf{erf}[(y-a)/\sqrt{2}D])/2\mathbf{erf}(a\sqrt{2}D))$ and $g(x)=\exp(-x^2/2D^2)$. The notation '**erf**' denotes the error function. The refractive index of the diffused channel, which has been divided into two different parts with the jump at $y=0$, under current investigation involves the coefficients specified at $a=3\,\mu$m, $D=3.35\,\mu$m, $\lambda=1.3\,\mu$m, $n_c=1.0$, $n_s=2.203$ and $\Delta n=0.01091$.

Subject to an incident light source, wave propagating in the diffused channel with the refractive index described above will be predicted. In Table I, the magnitudes of $k_0 n_{\mathrm{e}}$ predicted at different grids agree well with 10.666679 shown in [10]. In addition, the predicted amplitude profile in Figure 3 is also seen to have the similar profile predicted in the work of [8]. We plot in Figure 4

DOI: 10.1002/fld

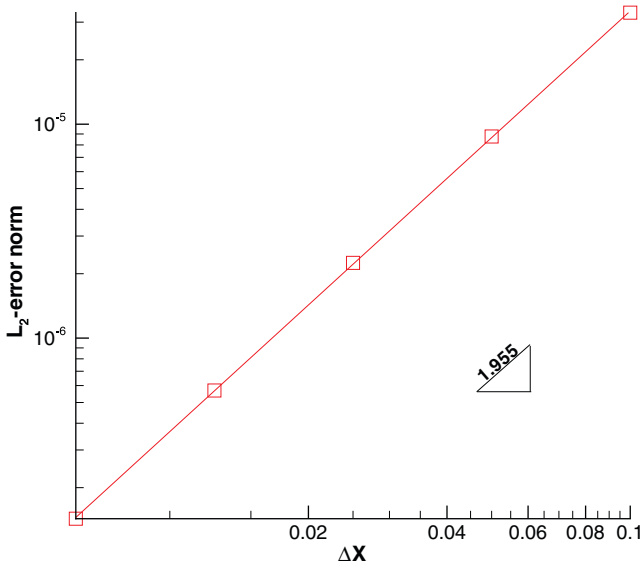

Figure 1. The predicted spatial rate of convergence for the two-dimensional analytic test problem chosen for the validation sake.

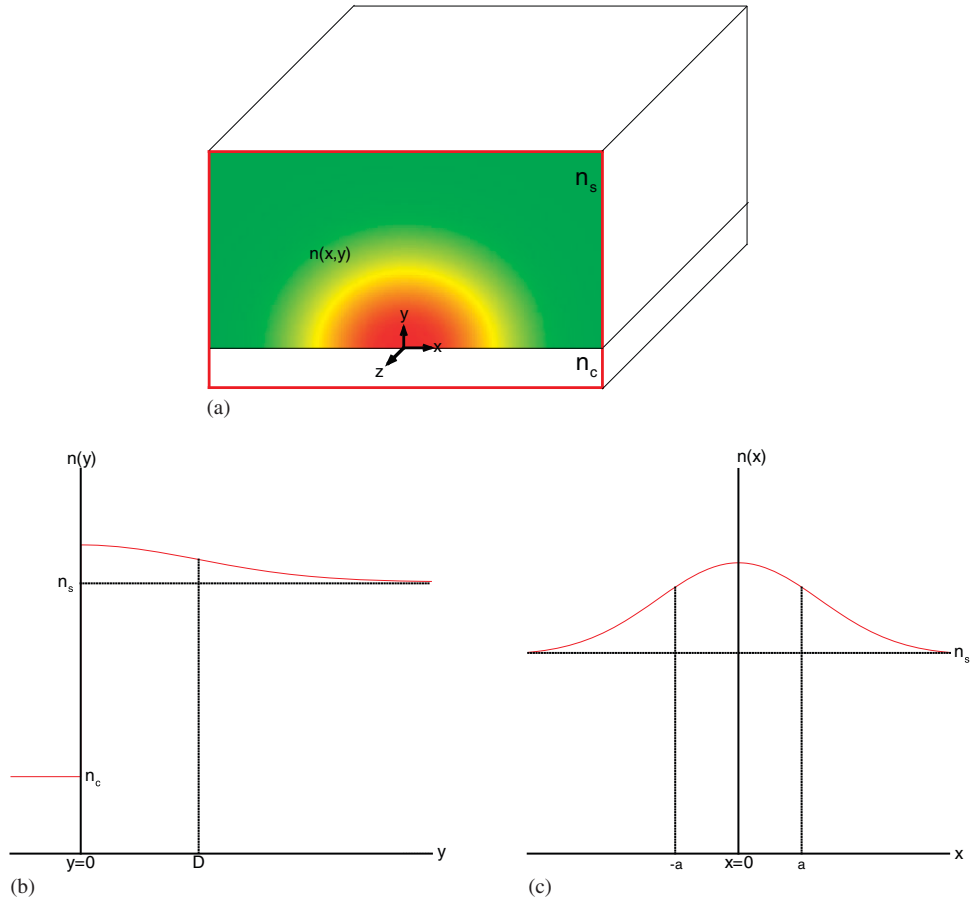

Figure 2. The refractive index profile for the diffused channel waveguide considered in the result section: (a) schematic of the waveguide structure and the refractive index profile; (b) plot of the computed value of n along the y-axis at $x=0$; and (c) plot of the computed value of n along the x-axis at $y=0$.

DOI: 10.1002/fld

Table I. The propagation constants predicted at different grids for the diffused channel waveguide schematic in Figure 2.

	$k_0 n_e$
$M=20,\ N=12$	10.6729059871051
$M=40,\ N=24$	10.6695968029455
$M=80,\ N=48$	10.6679630380804
$M=120,\ N=72$	10.6674623979537
$M=160,\ N=96$	10.6672313273201
$M=170,\ N=102$	10.6671923498354

The computed value of $k_0 n_e$ in [10] is 10.666679.

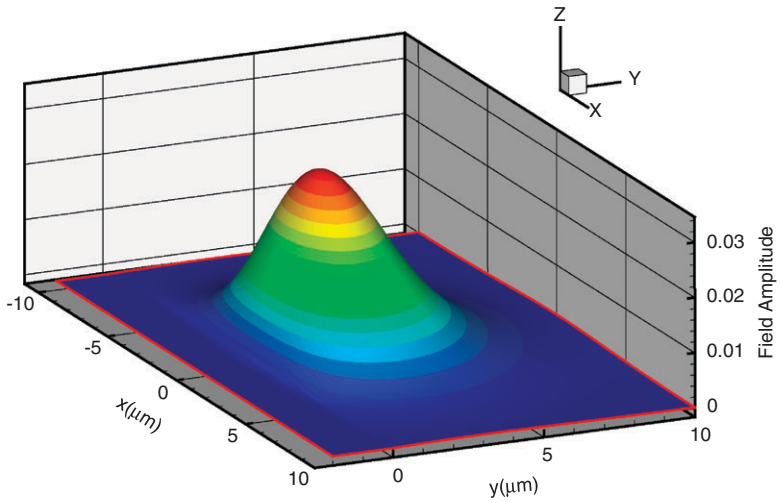

Figure 3. The predicted field intensity for the investigated diffused channel waveguide problem schematic in Figure 2.

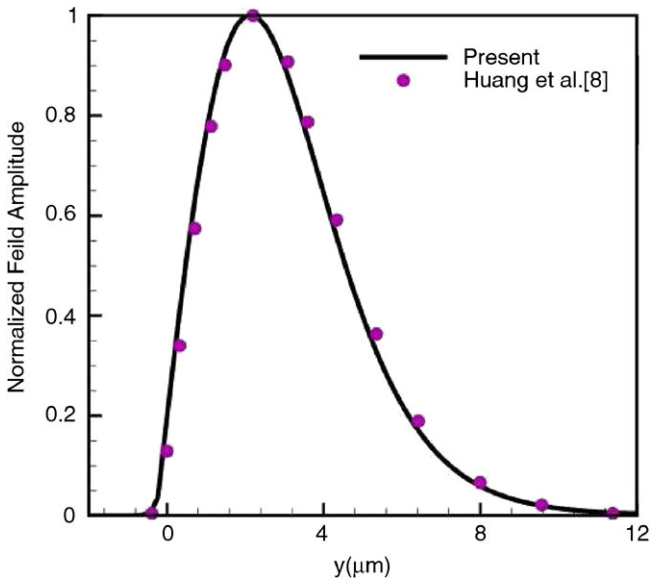

Figure 4. The predicted field intensity for the investigated diffused channel waveguide problem schematic in Figure 2.

DOI: 10.1002/fld

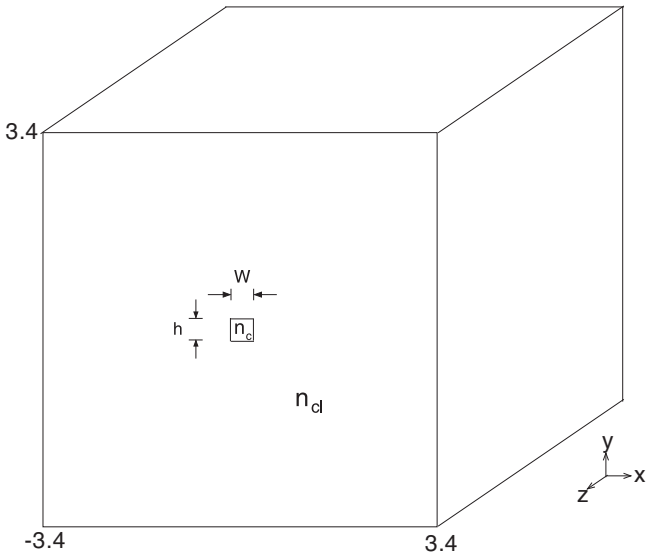

Figure 5. Schematic of the three-dimensional rectangular optical waveguide with $n_{cl}=2.19$, $n_c=3.50$, $W=0.4\,\mu\text{m}$ and $h=0.4\,\mu\text{m}$.

Table II. The predicted effective refractive indices of the semi-vector field for the rectangular optical waveguide schematic in Figure 5.

	$n_{\text{e,present}}$	$\lvert n_{\text{e,present}}-n_{\text{e,ref}}\rvert$
$M=17,\ N=17$	3.22931350761208	1.2113507E−2
$M=34,\ N=34$	3.21574190359676	1.4580970E−3
$M=68,\ N=68$	3.21688807797960	3.1192300E−4

The value of $n_{\text{e,ref}}$ in [11] is 3.2172. Note that the computed values of n_{e} are not monotonically decreased while the computed difference between the currently predicted and the referenced values are monotonically smaller with the increasing number of nodes. The rate of convergence is 2.3019.

Table III. The predicted effective refractive indices of the full-vector field for the rectangular optical waveguide schematic in Figure 5.

	$n_{\text{e,present}}$	$\lvert n_{\text{e,present}}-n_{\text{e,ref}}\rvert$
$M=25,\ N=15$	1.42239106123268	3.705039E−3
$M=50,\ N=30$	1.42418047664807	1.915624E−3
$M=75,\ N=45$	1.42524088728935	8.552130E−4

The value of $n_{\text{e,ref}}$ is 1.4260961 [12].

the computed normalized field amplitude along the y-axis at $x=0$. It can be seen that our currently predicted results agree well with the spectral solution given in [8].

We then solve the full-vector and semi-vector field equations in the rectangular waveguide schematic in Figure 5. The semi-vector wave simulation is carried out at $n_c=3.5$, $n_{cl}=2.19$, $W=0.4\,\mu\text{m}$, $h=0.4\,\mu\text{m}$ and $\lambda=1.55\,\mu\text{m}$. As for the analysis of full-vector field equations, we consider the case with $n_c=1.5$, $n_{cl}=1.0$, $W=3\,\mu\text{m}$, $h=1.55\,\mu\text{m}$ and $\lambda=1.55\,\mu\text{m}$. The computed effective refractive indices tabulated in Tables II and III for the semi-vector and full-vector fields,

DOI: 10.1002/fld

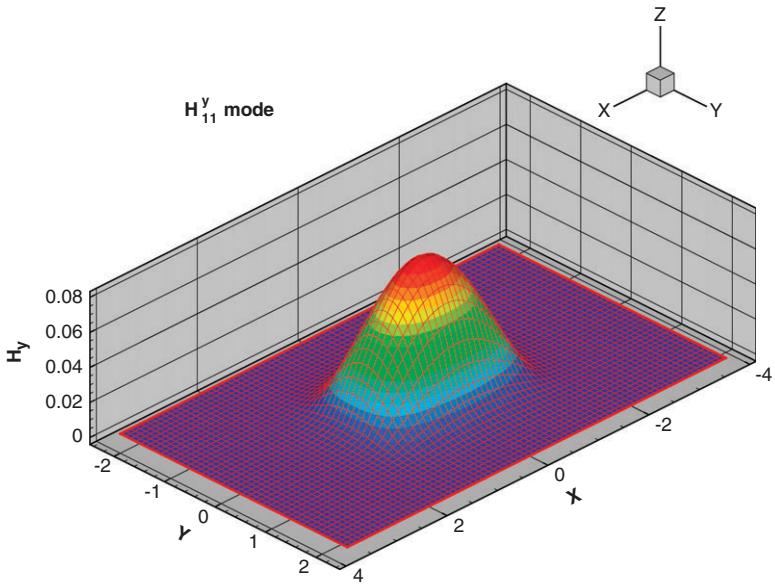

Figure 6. The predicted field intensity H_{11}^{y} for the rectangular optical waveguide schematic in Figure 5.

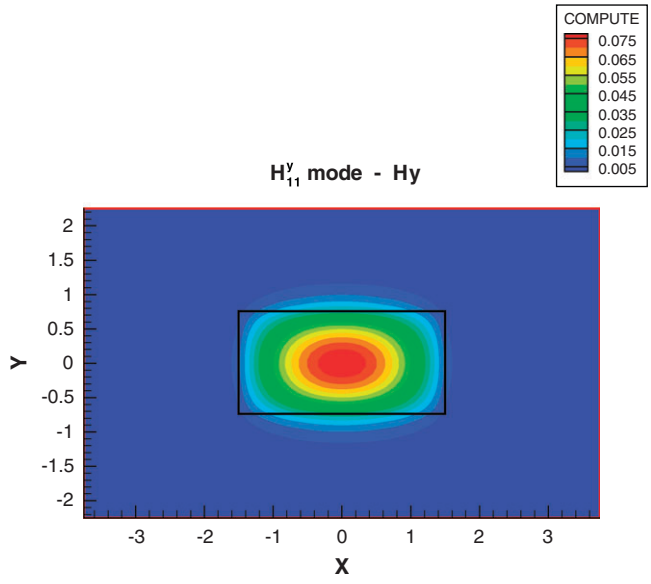

Figure 7. The predicted field intensity H_{11}^{y} for the rectangular optical waveguide schematic in Figure 5.

respectively, are both agreed well with the predicted values tabulated in [11, 12]. Note that the computed values of n_e are not monotonically distributed. The difference between the computed and the reference values of effective refractive index decreases, however, with the increase of mesh points. We also plot the H_{11}^{y} mode field amplitudes for the full-vector problem in Figures 6 and 7.

We then proceeded to analyze the optical wave propagation in a geometrically more complex waveguide schematic in Figure 8 by solving the full-vector waveguide equations at $n_c = 3.44$, $n_s = 3.4$, $n_a = 1.0$, $W = 3\,\mu m$, $h = 0.5\,\mu m$, $t = 0.5\,\mu m$ and $\lambda = 1.55\,\mu m$. The predicted effective refractive index n_e, tabulated in Table IV, agrees again well with the predicted value given in [12]. The amplitude for H_{11}^{y} is plotted in Figures 9 and 10.

DOI: 10.1002/fld

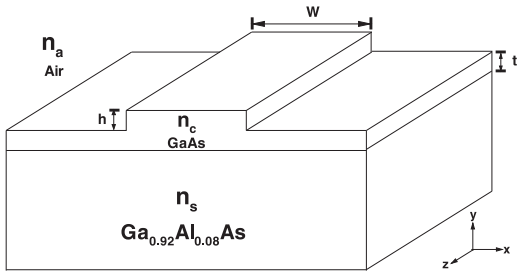

Figure 8. Schematic of the semiconductor rib optical waveguide with $n_s = 3.40$, $n_c = 3.44$, $n_a = 1.0$, $W = 3\,\mu\text{m}$, $h = 0.5\,\mu\text{m}$ and $t = 0.5\,\mu\text{m}$.

Table IV. The predicted effective refractive indices for the semiconductor rib optical waveguide schematic in Figure 8.

	n_e	$\lvert n_e - n_{e,exact}\rvert$
$M = 36,\ N = 24$	3.41154634822330	1.601252E−3
$M = 54,\ N = 36$	3.41195189416494	1.195706E−3
$M = 72,\ N = 48$	3.41221249715367	9.351030E−4

The value of n_e is 3.4131476 [12].

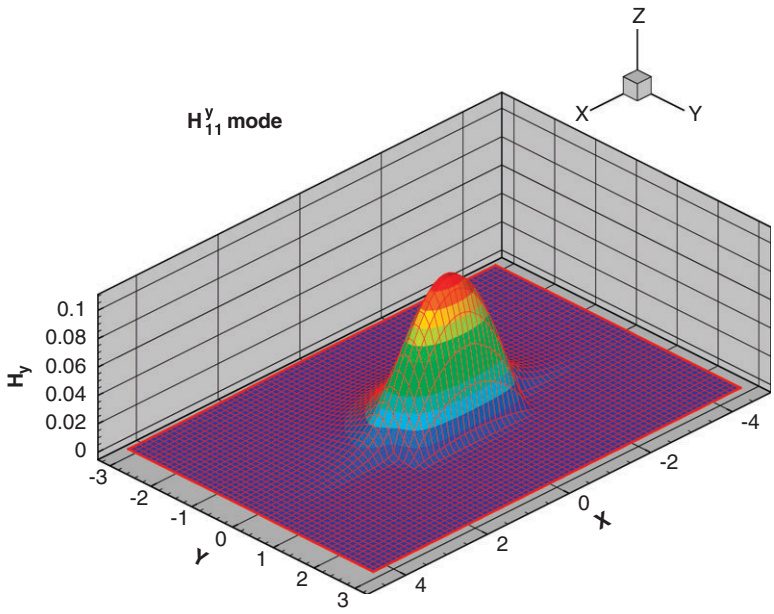

Figure 9. The predicted field intensity H_{11}^{y} for the rib optical waveguide schematic in Figure 8.

6. CONCLUDING REMARKS

We have proposed in this study the CDR finite difference scheme to solve Maxwell's equations in frequency domain. The three-dimensional waveguide equations have been investigated within the full-vector and semi-vector frameworks. All the predicted results have been shown to be compared

DOI: 10.1002/fld

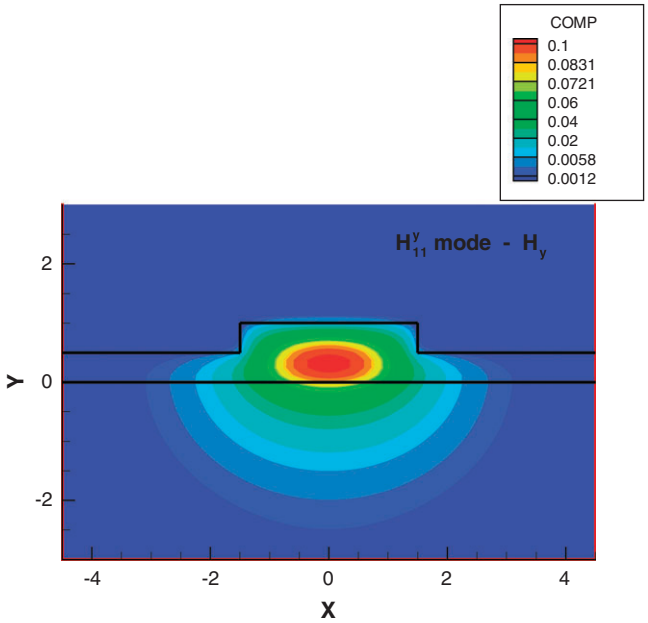

Figure 10. The predicted field intensity H_{11}^{y} for the rib optical waveguide schematic in Figure 8.

well with the benchmark solutions of the three-dimensional waveguides investigated at different optical properties.

ACKNOWLEDGEMENTS

The financial supports provided by the National Science Council under the grants NSC97-2221-E-002-250-MY3 and CQSE project 97R0066-69 are gratefully acknowledged. Computational hardwares from the National Center of High-performance Computing (NCHC) and the Computer Center of National Taiwan University are also highly appreciated.

REFERENCES

1. Feit MD, Fleck JA. Computation of mode properties in optical fiber waveguides by a propagating beam method. *Applied Optics* 1980; **19**:1154–1164.
2. Liu Y. Fourier analysis of numerical algorithms for the Maxwell equations. *Journal of Computational Physics* 1996; **124**:396–416.
3. Sanz-Serna JM, Calvo MP. *Numerical Hamiltonian Problems*. Chapman & Hall: London, NY, 1994.
4. Anderson N, Arthurs AM. Helicity and variational principles for Maxwell's equations. *International Journal of Electronics* 1983; **54**:861–864.
5. Johnson SG, Joannopoulos JD. Block-iterative frequency-domain methods for Maxwell's equations in a plane wave basis. *Optics Express* 2001; **8**(3):173–190.
6. Cockburn B, Li F, Shu CW. Locally divergence-free discontinuous Galerkin methods for the Maxwell equations. *Journal of Computational Physics* 2004; **194**:588–610.
7. Jiang BN, Wu J, Povinelli LA. The origin of spurious solutions in computational electromagnetics. *Journal of Computational Physics* 1996; **125**:104–123.
8. Huang CC, Huang CC, Yang JY. An efficient method for computing optical waveguides with discontinuous refractive index profiles using spectral collocation method with domain decomposition. *Journal of Lightwave Technology* 2003; **21**(10):2284–2296.
9. Sheu TWH, Lin RK, Liu GL. Development of a continuity-preserving segregated method for incompressible Navier–Stokes equations. *Computer Methods in Applied Mechanics and Engineering* 2006; **196**:502–515.
10. Sharma A, Bindal P. Variational analysis of diffused planar and channel waveguides and direction couplers. *Journal of the Optical Society of America A* 1994; **11**:2244–2248.
11. Kawano K, Kitoh T. *Introduction to Optical Waveguide Analysis*: *Solving Maxwell's Equation and the Schrödinger Equation*. Wiley: New York, NY, 2001; 160.
12. Huang CC, Huang CC, Yang JY. A full-vectorial pseudospectral modal analysis of dielectric optical waveguides with stepped refractive index profiles. *IEEE Journal of Selected Topics in Quantum Electronics* 2005; **11**(2):457–465.

DOI: 10.1002/fld